Journal of Materials Chemistry A

Accepted Manuscript

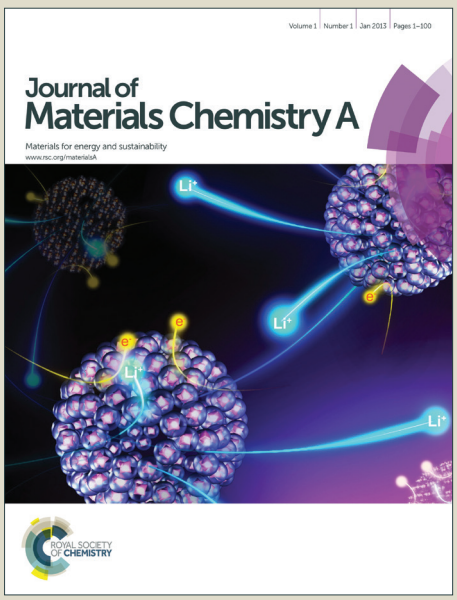

ROYAL SOCIETY OF CHEMISTRY

www.rsc.org/materialsA

A table of contents

**Colour graphic*

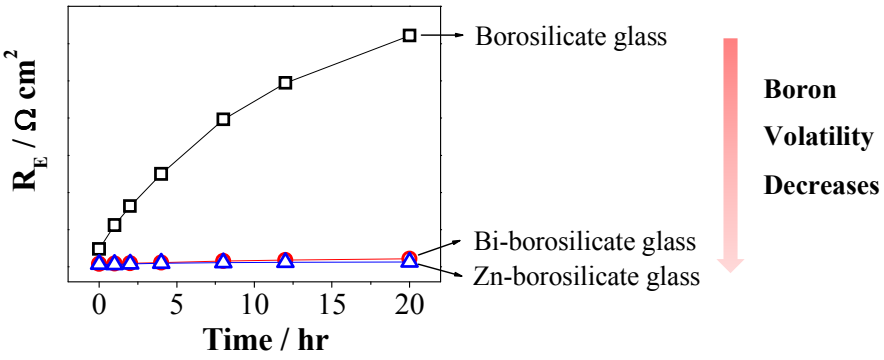

**Text*

Bismuth and zinc doping significantly suppresses boron volatility of borosilicate sealants and minimizing boron poisoning of cathodes of SOFCs.

New zinc and bismuth doped glass sealants with substantially suppressed boron deposition and poisoning for solid oxide fuel cells

Kongfa Chen,[ab] Lihua Fang,[a] Teng Zhang,[a,*] San Ping Jiang [b,*]

[a] College of Materials Science and Engineering, Fuzhou University, Fuzhou, Fujian 350108, China

[b] Fuels and Energy Technology Institute & Department of Chemical Engineering, Curtin University, Perth, WA 6102, Australia

Abstract

Borosilicate-based glasses are the most common sealant material of solid oxide fuel cells (SOFCs). However, boron species vaporized from glass sealants poison and degrade the electrocatalytic activity of cathodes of SOFCs. In this study, we report the development of new class of glass sealants based on bismuth and zinc doped borosilicates with significantly suppressed boron volatility. Doping Bi induces the $[BO_3]\rightarrow[BO_4]$ transition with increased binding energy of boron, while addition of Zn leads to the formation of boron-containing compound, $Sr_3B_2SiO_8$ with significantly increased stability of boron in the glass matrix. Using $La_{0.6}Sr_{0.4}Co_{0.2}Fe_{0.8}O_3$ **(**LSCF) perovskite oxide as the cathode to assess the boron deposition and poisoning, the results indicate that the polarization performance of LSCF cathode for the O_2 reduction reaction in the presence of Bi and Zn doped glass is very stable with negligible change in the microstructure of the electrodes. In contrast, in the case of conventional borosilicate glass, boron preferentially deposits at the electrode/electrolyte region under cathodic polarization, forming primarily $LaBO_3$, disintegrating the perovskite structure and significantly degrading the electrochemical activity of the LSCF cathodes. Doping Bi or Zn remarkably reduces the boron volatility of the glass, thus effectively inhibiting the poisoning of boron species on the microstructure and electrocatalytic activity of

*Corresponding author. Tel.: +61 8 9266 9804; fax: +61 8 9266 1138; E-mail: s.jiang@curtin.edu.au (S.P. Jiang); Tel.: +86 591 22866540; fax: +86 591 22866537; *Email address*: teng_zhang@fzu.edu.cn (T. Zhang).

SOFC cathodes such as LSCF. The present results demonstrate for the first time that the Bi and Zn doping is the most effective strategy to minimizing the boron poisoning from the source by suppressing the boron vaporization of borosilicate-based glass sealant materials.

Keywords: Solid oxide fuel cells; Borosilicate glass sealants; Boron poisoning; Bismuth and zinc doping; Suppressed boron volatility.

1. Introduction

Electricity is the most convenient form of energy today. For the past one hundred years, electricity is primarily produced by combustion of fossil fuels which has an intrinsically low conversion efficiency and emits carbon dioxide and other air pollutants. Carbon dioxide contributes to climate changes. With increasing energy demand, depleting fossil fuel reserves, and growing concern about the climate and environment, there is an urgent need to increase electricity generation efficiency and to develop renewable energy sources. Solid oxide fuel cell (SOFC) is an energy conversion device to electrochemically convert the chemical energy of fuels such as hydrogen, methanol, ethanol, natural gas, and hydrocarbons to electricity, and is considered to be the most efficient energy conversion technology. SOFCs can be classified into tubular and planar designs, and the planar design is more favored in terms of its advantages such as higher cell power densities, and lower manufacturing cost.[1, 2] In the case of planar SOFCs, it is essential to use a hermetic seal such as borosilicate-based glass and glass-ceramics to separate the fuels supplied to the anode and the air to the cathode.[3-8] Boron additives in the glass play an important role to tailor its physical properties such as viscosity and softening temperature.[9] One of the significant challenges of borosilicate glass-based sealant materials is the high volatility of boron species under SOFC operating conditions, forming BO_2 (g) under dry conditions and $B_3H_3O_6$ (g) under wet, reducing conditions.[9] Studies have shown that volatile boron species have a significant poisoning effect on the

electrochemical activity of SOFC cathodes such as (La,Sr)MnO_3 (LSM) and (La,Sr)(Co,Fe)O_3 (LSCF).[10-13]

Recently, we studied in details the effect of volatile boron species on the microstructure and electrochemical activity of SOFC cathodes such as LSM and LSCF.[14-18] Boron is chemically reactive with the LSM and LSCF electrode materials, significantly degrading the microstructure and forming insulating borate phases. In the case of conventional LSM electrodes, the reaction between boron and LSM occurs primarily on the surface. However, the volatile boron species has a significant detrimental effect on the microstructure and electrochemical activity of nano-structured LSM-YSZ cathodes, leading to the decomposition of LSM perovskite structure and the significant degradation of the electrocatalytic activity of the electrode.[14] In the case of LSCF, volatile boron species is very reactive, forming $LaBO_3$ and Fe_2O_3. The interaction between the volatile boron species and LSCF electrodes leads to the significant change in the microstructure and degrades dramatically the electrocatalytic activity of conventional LSCF and nano-structured LSCF infiltrated $Gd_{0.1}Ce_{0.9}O_{1.95}$ (LSCF-GDC) electrodes.[15] The results show that boron has a higher reactivity with LSCF as compared to LSM.[16] In addition to the electrode materials, boron is also chemically incompatible with SOFC electrolyte materials such as Y_2O_3-ZrO_2 and GDC.[19]

Extensive efforts have been made on the effect of composition and additives on the thermal, chemical, mechanical, and electrical properties of glass-based sealant materials in order to seal cell components and to reach stable operation for 10,000 to 40,000 h at 500-1000 ^oC in oxidizing and reducing atmospheres and withstand numerous thermal cycles between room and cell operating temperatures.[3, 7, 20-22] However, very few studies are on the effect of the additives and doping on the volatility of the glass components in particular boron species and thus to eliminate or minimize the adverse effect of volatile species on the performance degradation of SOFCs. In this study, we report the development of new bismuth

(Bi) and zinc (Zn) doped borosilicate glass with substantially suppressed boron volatility for SOFCs. The excellent stability of the glass in terms of the boron volatility has been tested on LSCF cathode. High sensitivity of LSCF to the boron poisoning[15, 19] makes LSCF an ideal candidate to assess the boron volatility of the borosilicate-based glass sealant materials, similar to the use of LSM electrode to assess the chromium volatility of chromia-forming metallic interconnect under SOFC operating conditions.[23] The results show that the LSCF electrode is very stable in the presence of Bi and Zn doped glass, demonstrating the great potential of the new glass sealants in the development of SOFC technologies with high performance and high durability.

2. Experimental

2.1. LSCF cathode and glass sealant preparation

In this work, $La_{0.6}Sr_{0.4}Co_{0.2}Fe_{0.8}O_3$ (LSCF, Fuel Cell Materials) electrodes were used to assess the effect of deposition and poisoning of the volatile boron species of the glass sealant material. The electrolyte pellets were prepared by pressing $Gd_{0.1}Ce_{0.9}O_{1.95}$ powder (GDC, AGC Seimi Chemical Co Ltd, Japan), followed by sintering at 1450 ^oC for 5 h. LSCF electrodes were applied on GDC electrolytes by slurry coating and sintered at 1000 ^oC for 2 h. The cathodes had a thickness of 6-30 μm and an electrode area of 0.5 cm^2.

The composition of bismuth and zinc doped $CaO–SrO–B_2O_3–SiO_2$ glasses is given in Table 1. In the table, G0 is the conventional $CaO–SrO–B_2O_3–SiO_2$ borosilicate glass without Bi and Zn additives, GB is the borosilicate with addition of 2 mol% Bi_2O_3 and GZ is the glass with 16 mol% ZnO. In all three glass compositions, the composition of B_2O_3 is more or less the same 7-8 mol%. A 50 g sample of each glass was prepared by melting a homogeneous mixture of reagent grade alkaline earth carbonates, boric acid, and various oxides in a platinum crucible in air at 1300-1500^oC for 1 h. Some of the melt was poured into stainless

steel mold to obtain cylindrical shaped glass specimens (25 mm in length and 6 mm in diameter) and the rest of the melt was quenched on a steel plate. Glass powders were then crushed and sieved to a particle size of 45 to 53 μm.

2.2 Glass characterization

The onset crystallization temperature (T_x) of glass powders was determined using differential scanning calorimetry (SDTQ600, TA Inc.) at a heating rate of 5 ºC min^{-1}. The coefficient of thermal expansion (CTE, between 200 and 600 ºC), glass transition temperature (T_g) and softening temperature (T_d) of quenched glass samples were determined by dilatometer (DIL402C, NETZSCH Inc.) at 5 ºC min^{-1} in air. CTE of glass samples after the heat-treatment at 700°C for 500 h was also measured. Raman spectra of quenched glass powders were collected in 200-1600 cm^{-1} wave number range by Raman spectrometer (Renishaw Invia). The light source was 514.5 nm argon laser with 10 seconds of exposure time. The O1s and B1s XPS spectra of quenched glass samples were obtained by X-ray photoelectron spectroscopy (ESCALAB 250, Thermo Scientific Inc.) using a monochromatic Al Kα source (10 mA, 15 kV). The phase and crystallinity of glass samples after the heat-treatment at 700 ^oC for 2 and 500 h were also examined by X-ray diffractometry (XRD, Bruker D8 Advance Diffractometer).

2.3. Electrochemical characterization

The glass powders were prepared into glass cylinders with a hole in the center and heat-treated at 750^oC for 2 h. The purpose of the central hole is to facilitate the air flow for the O_2 reduction reaction. The as-prepared glass cylinder was cut into pellets with ~4.0 mm in thickness and ~9 mm in diameters by a diamond saw, and the diameter of the central hole was 1.6 mm. Glass pellet was placed on top of the LSCF cathodes separated with a Pt mesh to prevent the direct contact between the cathode and glass pellet. In this way, volatile boron species can only deposit on the cathode via gas phase diffusion. Pt meshes were used as

current collector of LSCF cathode. Fig. 1 shows the schematic diagram of the experimental setup.

Polarization was carried out under cathodic current passage at 200 mA cm^{-2} and 700^{o}C for 20 h, with an industrial grade air at a flow rate of 100 ml min^{-1}, and impedance responses were recorded under open circuit using a Gamry Reference 3000 Potentiostat. The impedance responses were measured at an amplitude of 10 mV from 0.1 Hz to 100 kHz. The electrode ohmic resistance (R_Ω) was obtained from the intercept on high frequencies, and electrode polarization resistance (R_E) was obtained by the differences of the intercepts between the low and high frequencies. For comparison, LSCF cathodes were also measured in the absence of glass pellets.

Electrode microstructure was examined with scanning electron microscopy (SEM, Neon 40EsB). The phase of the cathodes before and after the heat-treatment was characterized by XRD.

3. Results and discussion

3.1. Characterization of glass sealants

Figure 2 is the thermal expansion curves of quenched glass samples. The coefficient of thermal expansion (CTE) of quenched glasses ranges from 12.2 to 13.3×10^{-6} K^{-1}. Similarly, the CTE of glass samples held at 700°C for 500 h was also measured, ranging from 10.4 to 12.7×10^{-6} K^{-1}. The CTEs of quenched glasses and glasses after heat-treatment for long period of time fall within the design range of SOFC glass sealants.[24] This indicates that borosilicate glasses with and without Bi and Zn doping are applicable as sealants for SOFCs. The glass transition temperature and softening temperature of glasses decrease with the addition of Bi_2O_3 as well as ZnO. The onset crystallization temperature of Bi doped glass, GB is 856^{o}C, higher than 794 and 769^{o}C for original glass, G0, and Zn doped glass, GZ, respectively.

Thermal properties of glass samples, including T_x, T_g, T_d and CTE, are summarized in Table 2.

Fig. 3a is Raman spectra of quenched glass samples. The deconvoluted Raman spectra of glasses are given in Fig. 3b to 3d (see Table S2, Support Information for the assignments of deconvoluted peaks). The peak at 261 cm^{-1} in glass GB (Fig. 3c) can be assigned for Bi-O bond in [BiO_3] unit,[25] whereas the peak at 256 cm^{-1} in glass GZ (Fig. 3d) corresponds to the Zn-O tetrahedral bending vibration of [ZnO_4] unit.[26, 27] In addition, the peak at 498 cm^{-1} in the FT-IR spectra of GB is associated with the stretching vibrations of Bi–O bonds in [BiO_6] units[28-30] (see Fig. S1 and Table S1, Support Information). This indicates that Bi_2O_3 and ZnO are incorporated into the network of borosilicate glass. In addition, the peaks at ~780 cm^{-1} can be ascribed to [BO_4] stretching vibration[28, 31, 32] and the peaks ranging from 1398 to 1449 cm^{-1} correspond for the vibration of B-O^- bond in [BO_3] unit.[31] It is worth noting that the ratios of integrated peak between [BO_4] and [BO_3] are 0.5, 1 and 0.08 for glass G0, GB and GZ, respectively. The increase in [BO_4]/[BO_3] ratio from glass G0 to GB indicates a [BO_3]→[BO_4] transition with the addition of Bi_2O_3. Such transition is not due to the presence of 7% Al_2O_3 in the glass GB as it is well known that the Al_2O_3 (<10 mole%) is added as network former in glasses and contributes to the [BO_4]→[BO_3] transition.[33, 34] The decrease in [BO_4]/[BO_3] ratio from glass G0 to GZ implies a [BO_4]→[BO_3] transition with the addition of ZnO.

Fig. 4 is the B1s XPS spectra of quenched glass samples. It is clear that the B1s binding energy (BE) in glasses increases from 191.9 eV for glass G0 to 192.9 eV for GB (Fig. 4a), in good agreement with the [BO_3]→[BO_4] transition in the Bi_2O_3 doped glass (Fig. 3c). The BE of B1s in GZ is 191.5 eV, very close to 191.9 eV of G0. This indicates that the [BO_4]→[BO_3] transition due to the ZnO doping in borosilciate glass has little effect on the binding energy of boron.

On the other hand, the O1s XPS curves can be deconvoluted into two peaks with different binding energies, i.e., non-bridging oxygen and bridging oxygen, respectively (see Fig.4b). The fraction of bridging oxygen can be calculated by comparing the integrated areas of two peaks and thus provides useful information on the overall network connectivity of glass.[29, 32] The fraction of bridging oxygen in GB is 84%, higher than 72% and 54% observed on glass G0 and GZ, respectively. Therefore, Bi_2O_3 in glass GB acts as a network former,[35] which contributes to the condensed network of glass and this explains the increase in onset crystallization temperature of GB (Table 2). In particular, Bi_2O_3 induces the $[BO_3]\rightarrow[BO_4]$ transition in the glass, which is consistent with the progressive conversion of $[BO_3]$ units to $[BO_4]$ units with increasing Bi_2O_3 content in B_2O_3-Bi_2O_3-ZnO glasses.[36] However, ZnO acts as a network modifier in glass GZ, which results in a more opened glass network and consequently the decrease in onset crystallization temperature of glass. Inoue et al. also reported that the thermal stability against crystallization decreases with the substitution of ZnO for B_2O_3 in $xZnO{-}10Bi_2O_3{-}(90\text{-}x)B_2O_3$ glasses.[36]

The critical role of Bi and Zn additives in the stabilization of boron is investigated by XRD and the results are shown in Fig. 5 for the glass samples after heat-treatment at 700^{o}C for 2 and 500 h. In the case of the heat-treatment at 700^{o}C for 2 h (Fig. 5a), some crystalline phases such as Sr_2SiO_4 and $CaSiO_3$ in G0, and Sr_2SiO_4, $Sr_3B_2SiO_8$ and $Ca_2ZnSi_2O_7$ in GZ can be observed, whereas GB remains in amorphous state. The XRD patterns of glass samples after the heat-treatment at 750^{o}C for 2 h used in the glass pellets preparation process are similar to that heat-treated at 700 ^{o}C (Fig. S2, Supporting Information). This indicates that the addition of Bi_2O_3 improves the thermal stability against crystallization of glass, consistent with the increase in network connectivity of GB (Fig. 4b). On the other hand, after the heat-treatment at 700^{o}C for 500 h, there are crystalline phases such as Sr_2SiO_4, $CaSiO_3$, $Ca_2SrAl_2O_6$ and $BiBO_3$ formed in GB glass, while the crystalline phases remain stable in G0

and GZ after the prolonged heat-treatment (Fig. 5b). This indicates that these crystalline phases in G0 and GZ are beneficial for the thermochemical properties of glass-ceramic sealants and the amorphous phase of GB glass will transfer to crystalline phase after prolonged heat-treatment at 700 ^{o}C.

After the heat-treatment at 700^{o}C for 2 h the crystalline content in glasses calculated by Rietveld method is 45 and 93% for G0 and GZ, respectively. In the case of the heat-treatment at 700^{o}C for 500 h, the main phase in the G0, GB, and GZ glasses is Sr_2SiO_4, $CaSiO_3$, and $Ca_2ZnSi_2O_7$, respectively (Table 3). Sr_2SiO_4 and $Ca_2ZnSi_2O_7$ have a desirable CTE of 11~12×10^{-6} and α_a=10.6×10^{-6}/α_c=20.2×10^{-6} K^{-1}, respectively,[37, 38] and they are known to be thermomechanical stable phases for glass-ceramic sealants. $CaSiO_3$ also has a low CTE of 9.4×10^{-6} K^{-1},[39] and the increase of its content from 13 wt% in G0 to 70 wt% in GB, leads to the decrease in CTE of GB glass from 12.7 to 10.4×10^{-6} K^{-1} after the heat-treatment at 700 ^{o}C for 500 h. In addition, the formation of boron-containing phases such as 5% $BiBO_3$ in GB and 7% $Sr_3B_2SiO_8$ in GZ also indicates that boron would be much more stable in the Bi_2O_3 and ZnO-doped borosilicate glasses, as compared to the boron in undoped borosilicate glass.

3.2. Boron deposition and poisoning of LSCF cathodes

The volatility of gaseous boron species of the glass samples was assessed by the electrochemical behaviour of LSCF electrodes. Fig. 6 is the polarization curves for the O_2 reduction reaction on LSCF cathodes measured at 200 mA cm^{-2} and 700^{o}C in air. For the reaction in the absence of glass, the LSCF electrode shows a very high activity and good stability during the polarization for 20 h (Fig. 6a). The initial R_Ω and R_E were 1.8 and 0.32 Ω cm^2, respectively, and reached 1.89 and 0.36 Ω cm^2 after polarized for 20 h. The low and very stable R_Ω and R_E for the O_2 reduction reaction on LSCF are clearly due to its high mixed ionic and electronic conductivity.[40-44] On the other hand, the electrocatalytic activity of the LSCF electrode degrades significantly in the presence of undoped glass, G0. The initial R_Ω

and R_E for the O_2 reduction reaction on LSCF in the presence of G0 glass were 2.7 and 2.4 Ω cm^2, respectively (Fig.6b). After polarized for 20 h, it increased rapidly to 13 and 31 Ω cm^2, almost 5 and 13 times of the initial value. The remarked increase in both R_Ω and R_E for the reaction on LSCF electrode is evidently due to the deposition and poisoning of volatile contaminants from the G0 glass. Our previous study has shown that the boron species from the borosilicate glass is chemically incompatible with the LSCF, and the interaction leads to significant activity deterioration of the LSCF cathodes.[15, 19] The much higher initial R_E of 2.4 Ω cm^2 as compared to 0.32 Ω cm^2 of the electrode in the absence of glass indicates that the deposition and poisoning of the volatile boron species occurs under open circuit conditions.

However, in the presence of Bi and Zn doped borosilicate glass (GB and GZ), the electrode degradation is substantially reduced (Fig. 6c and d). The initial R_E before the polarization in the presence of GB and GZ glasses is 0.38 and 0.34 Ω cm^2, respectively, very close to 0.32 Ω cm^2 of the electrode in the absence of glass. This indicates the alleviated boron poisoning of the electrode activity before the polarization. Most important, the increase in the R_Ω and R_E is very small during the polarization. For example, for the reaction on LSCF in the presence of GZ glass, R_E is 0.65 Ω cm^2 after polarized for 20 h, much smaller than 31 Ω cm^2 measured on LSCF in the presence of G0 glass under identical test conditions. The much stable R_Ω and R_E value for the O_2 reduction reaction on the LSCF cathodes is a clear indication of the presence of a much low gaseous boron species vaporized from GB and GZ glasses.

Figure 7 is the impedance responses of the LSCF electrodes before and after the polarization for 20 h. For the polarization in the absence of glass, the initial impedance responses of LSCF electrode before the polarization are characterized by two arcs at high and low frequencies (Fig. 7a). The impedance arcs become overlapped after the polarization, but the change in the size of impedance responses is very small. On the other hand, the initial

electrode impedance for the reaction on LSCF cathode prior to the polarization in the presence of G0 is ~2.5 Ωcm^2, much greater than ~0.35 Ωcm^2 in the absence of glass (Fig. 7b). After polarized for 20 h, there is a substantial increase of the impedance arc, indicating the significant poisoning of boron species on the oxygen dissociation and surface diffusion processes.[18, 45] In the case of polarization in the presence of GB and GZ, the low frequency impedance arcs also experience an increase after the polarization for 20 h (Fig. 7c and d), but the increase is much smaller as compared to that in the presence of the G0 glass. The change in the R_E for the reaction on LSCF cathodes in the presence of GB and GZ glass is very small (Fig.7e), indicating the substantially reduced boron poisoning of the Bi and Zn-doped glasses.

3.3. Boron deposition and microstructure of LSCF cathodes

Figure 8 is the SEM micrographs of the surface and cross sections of the LSCF cathode/GDC electrolyte interface region before and after the polarization tests at 200 mA cm^{-2} and 700 ^oC for 20 h. The as-prepared LSCF electrode is porous with smooth particle surface, and the particle size is in the range of 200-700 nm (Fig. 8a and b). LSCF particles are in intimate contact with the GDC electrolyte. After the polarization in the presence of borosilicate glass, G0, there is a significant microstructure change particularly at the electrode/electrolyte interface (Fig. 8c and d). New particles with irregular shape distribute discretely on the surface (indicated by the arrows in Fig. 8c). The newly formed particles are in the range of 70-100 nm and have a very different morphology as compared to the host LSCF particles. At the interfacial region, the LSCF particles are completely covered by small particles (~20-50 nm) and plate-shaped particles in the size range of 100-200 nm (Fig. 9d). Such a dramatic change in the microstructure particularly at the interface region clearly indicates the deposition and reaction of volatile boron species from the borosilicate glass, consistent with the previous study of the boron deposition and poisoning on the dense LSCF bar samples.[18, 19] The electrode thickness was ~28 μm in this case and as shown below, the

thickness of the boron reaction layer is ~6 μm. On the other hand, there are no visible microstructure changes on the electrode surface and at the interface region for the LSCF electrodes after polarized in the presence of Bi and Zn doped borosilicate glass, GB and GZ (Fig. 9e-h). The morphology of the LSCF electrodes after polarization in the presence of GB and GZ glass is essentially the same as that of as-prepared LSCF. This implies that the Bi and Zn doping substantially suppressed the vaporization of boron species under the SOFC operating conditions at 700 ^{o}C. The much clean microstructure of the LSCF electrode in the presence of GB and GZ glasses is in excellent agreement with its very stable polarization behaviour as shown in Figs.6 and 7.

The effect of boron deposition and poisoning was examined on LSCF electrodes with different thickness. Fig. 9 is the SEM micrographs of cross sections of LSCF cathodes with different thickness after polarization at 200 mA cm^{-2} and 700 ^{o}C in the presence of G0 glass for 20 h. The electrode thickness was 28 μm and 6 μm, respectively. Similar to the thick LSCF electrode (28 μm), the electrode performance of the LSCF electrode with a reduced thickness of 6 μm was also deteriorated significantly in the presence of G0 glass (see Fig. S3, Supporting Information). For example, the initial R_E was 25 Ω cm^2 and increased substantially to 241 Ω cm^2 after polarization at 200 mA cm^{-2} and 700 ^{o}C for 20 h. There are significant changes in the microstructure of LSCF cathodes, characterized by the formation of two distinctive regions, Region I and II. Region I is the region close to the electrode/electrolyte interface with significant microstructure change. In the case of the 28-μm-thick LSCF electrode, Region I has a thickness of 6 μm (Fig. 9b). Two characteristic regions are also clearly visible in the case of 6-μm-thick LSCF cathode with the formation of a 2.5-μm-thick Region I at the interface region. Similar to that observed for the thick LSCF electrode, there is formation of large number of small particles in the range of 50-150 nm (Fig. 9e). The original and large LSCF particles no longer exist, indicating the disintegration

and decomposition of the LSCF perovskite structure. The complete change of the microstructure at the electrode/electrolyte interface region indicates the new phase formation clearly due to the attack by the volatile boron species.[15] On the other hand, the change in the electrode microstructure in Region II appears relatively small (Fig. 9f). This indicates that the boron deposition and poisoning for the O_2 reduction reaction on LSCF electrodes occur preferentially at the electrode/electrolyte interface region under the cathodic polarization conditions and is independent of the electrode thickness.

The microstructure of LSCF under open circuit at 700 ^{o}C for 20 h in the presence of G0 was also examined and the results are shown in Fig. 10. There is no formation of large number of small spherical particles and plates as observed on LSCF electrodes after polarization for 20 h (see Fig. 8d). However, the change in the microstructure of the LSCF electrodes after exposed to G0 glass under open circuit conditions is clearly visible. As compared to the original smooth LSCF particles of as-prepared LSCF electrode (Fig.8a and b), the surface of LSCF grains became rough at the electrode/electrolyte interface and on the electrode surface after exposed to G0 glass. There is a clear formation of irregularly shaped and small particles in the range of 50-80 nm (indicated by arrows in Fig.10). This indicates that boron deposition also occurs under open circuit conditions. However, there is no visible difference in the electrode/electrolyte interface region and on the electrode surface. This again confirms that the preferential deposition of boron at the electrode/electrolyte interface regions only occurs under the cathodic current polarization conditions. This is very different from the chromium deposition at the LSCF electrodes in the presence of chromia-forming alloy, where chromium deposition occurs preferentially on the electrode surface rather than at the electrode/electrolyte interface.[46-48]

Fig. 11 is the XRD patterns of thick and thin LSCF cathodes after polarized at 200 mA cm^{-2} and 700^{o}C for 20 h, in the presence of glass samples. In the case of the 28-µm-thick

LSCF cathode, there are characteristic and high intensity GDC and LSCF diffraction peaks originated from the electrolyte and electrode, respectively (Fig. 11a). The perovskite phase of LSCF does not change much after the polarization, though some very small additional XRD peaks were detected in the electrode after polarized in the presence of G0 glass. The small peaks were identified as originated from the new $LaBO_3$ phase. The very small XRD peaks of the $LaBO_3$ phase may be due to the thick Region II (22 µm, Fig. 9a). In the case of GB and GZ glass, no new phases were detected (Fig.11a), indicating the structural integrity of LSCF electrodes after polarization in the presence of Bi and Zn doped glass. This is consistent with the SEM results (Fig. 8 and 9). On the other hand, the XRD pattern of the 6-µm-thick LSCF electrode after polarized in the presence of G0 glass for 20 h shows significant new diffraction peaks in addition to the characteristic peaks originated from LSCF perovskite and GDC cubic phases. The new diffraction peaks were identified due to $LaBO_3$, Fe_2O_3 and/or $CoFe_2O_4$ phases. The formation of the new lanthanum borate phases indicates the chemical reaction between LSCF and volatile boron species from the G0 glass, leading to the destruction and decomposition of LSCF perovskite structure. The much stronger XRD signal of $LaBO_3$ in the case of the thin 6-µm-thick LSCF electrode as compared to the thick 28-µm-thick LSCF electrode also indicates that such structural destruction by boron poisoning occurs at the inner surface of the LSCF electrodes, in excellent agreement with the substantial microstructure change at the electrode/electrolyte interface (Region I, Fig. 9).

3.4. Effect of Bi and Zn doping on the boron volatility

The present study has demonstrated clearly that in the case of undoped borosilicate glass, G0, volatility of boron species is very high. The high volatile boron species is electrochemically verified by the substantial deterioration in the electrochemical activity of the LSCF cathodes in the presence of borosilicate glass under SOFC operation conditions. SEM and XRD results clear indicate that under cathodic polarization conditions, boron

deposition preferentially occurs at the electrode/electrolyte interface region. Boron deposition leads to the reaction between boron species and LSCF, decomposing the perovskite structure. The detection of lanthanum borate and not strontium borate phase at the electrode/electrolyte interface indicates that boron primarily reacts with lanthanum of the LSCF and the depletion of lanthanum would lead to the disintegration of the perovskite structure.

$$BO_2 + La_{0.6}Sr_{0.4}Co_{0.2}Fe_{0.8}O_{3-\delta} \rightarrow LaBO_3 + Fe_2O_3 + CoFe_2O_4 + SrO \quad [1]$$

This is consistent with the previous study of the reactivity between boron oxide and dense LSCF bar samples.[18, 19] The formation of distinctive Region I and II for the reaction on LSCF electrodes under the cathodic polarization conditions (Fig. 10) indicate that boron deposition and poisoning is not strictly limited at the electrode/electrolyte interface. The measurable thickness of Region I (i.e., 6 µm in the case of 28 µm-thick LSCF and 2.5 µm in the case of the 6 µm-thick LSCF) indicates that boron reaction occurs in a finite reaction zone, close to the electrode/electrolyte interface. Wang et al also observed the deposition of sulphur species in the vicinity of LSCF electrode/GDC electrolyte interface, and they postulated that the high concentration of oxide ion vacancies at the electrochemically active region under the polarization conditions promoted the SO_2 adsorption and thereby $SrSO_4$ formation.[49]

In contrast to the situation in the presence of conventional borosilicate glass, the LSCF electrodes show a much stable polarization performance, no distinctive formation of reaction zone at the electrode/electrolyte interface and negligible microstructure change at the electrode surface and in the electrode bulk under cathodic polarization in the presence of Bi and Zn doped borosilicate glass, GB and GZ under identical experimental conditions. This indicates that the fundamental reason for the very stable electrode performance and negligible microstructure change of LSCF electrodes is the substantially suppressed boron vaporization of the doped glass. The detection of borates in the reaction zone of the LSCF electrodes in the presence of undoped borosilicate glass also implies that the main volatile contaminant species

of the borosilicate glass is boron.

Raman, XPS and XRD results (Fig.3-5) clearly demonstrate that boron elements in borosilicate are stabilized by different mechanisms in Bi and Zn doped borosilicate glasses. For the Bi-doped glass (GB), the $[BO_3] \rightarrow [BO_4]$ transition (Fig. 3c) contributes to the increase in the binding energy of boron (Fig. 4a) and thus the depressed boron vaporization from glass. The formation of boron-containing phase, $BiBO_3$ after heat-treatment at 700 ^oC for 500 h also indicates that Bi doping would increase the long-term stability of GB glass against boron vaporization. However, the significant depressed boron vaporization from glass with zinc doping can be attributed to the formation of boron-containing phase, i.e., $Sr_3B_2SiO_8$. A recent work of our group has revealed that the formation of boron-containing phase, e.g., SrB_2O_4, can be beneficial for the reduction of boron vaporization at 800^oC in wet reducing atmosphere, due to its much lower partial pressure compared with that of boron species in glass matrix (3.9×10^{-7} vs. 3.5×10^{2} Pa).[50] The significant boron deposition and poisoning of LSCF cathodes in the presence of conventional borosilicate glass, G0, indicates the high volatility of boron due to the fact that boron mainly exists in the $[BO_3]$ form with low binding energy, despite the partial crystallization upon heat-treatment. Bi and Zn doping substantially reduce the boron vaporization by stabilizing boron by forming more stable $[BO_4]$ form in the case of GB glass and by the formation of boron-containing phase, $Sr_3B_2SiO_8$ in the case of Zn-doped glass. In addition, studies have shown that the bismuth doping is beneficial to tune the properties of glass,[21, 51] and the addition of zinc is also of help to improve the mechanical properties and chemical durability of glass.[3, 52, 53]

4. Conclusions

We developed new glass sealants based on Bi and Zn doping of conventional $CaO–SrO–B_2O_3–SiO_2$ borosilicate glass with substantially reduced boron deposition and

poisoning for SOFCs. The Bi or Zn doping significantly suppressed the volatility of boron element of the glass and this is evidently confirmed by the very stable electrode performance and negligible microstructure change of LSCF cathodes after exposed to the Bi and Zn doped glasses under polarization at 200 mA cm^{-2} at 700^{o}C for 20 h. This is in contrast to the significant performance and microstructure degradation of LSCF cathodes after exposed to conventional borosilicate glass under identical experimental conditions. In the presence of conventional and undoped borosilicate glass, electrochemical activity of LSCF electrodes for the O_2 reduction reaction deteriorates very quickly. For example, R_E increased from 2.4 to 31 Ω cm^2 after polarization at 200 mA cm^{-2} and 700 ^{o}C for 20 h for the reaction. Under cathodic polarization conditions, boron deposition preferentially occurs at the electrode/electrolyte interface region, forming $LaBO_3$ and leading to the destruction of the perovskite structure.

Bi and Zn additives play a critical role in the stabilization of boron elements in borosilicate glasses. The Bi doping induces the $[BO_3] \rightarrow [BO_4]$ transition and therefore enhances the stability of boron in the network of glass GB due to the increased binding energy of boron. On the other hand, the Zn doping results in the formation of boron-containing phase ($Sr_3B_2SiO_8$) and thus dramatically reduces the boron vaporization from glass matrix. Bi and Zn doped glass materials show the promising potential as the advanced glass-based sealants for durable SOFCs by eliminating the boron deposition and poisoning of cathodes from the source. The present study also demonstrates that LSCF electrode is an ideal material to electrochemically assess the boron volatility of borosilicate-based glass sealant materials under SOFC operation conditions.

Acknowledgements

The project is supported by Curtin University Research Fellowships, Australian Research Council *Linkage Project funding scheme* (project number: LP110200281), Australia, the

National Natural Science Foundation of China (No. 51102045) and Program for New Century Excellent Talents in Fujian Province University (No. JA12013), China. The authors acknowledge the facilities, scientific and technical assistance of the Curtin University Electron Microscope Facility and Curtin X-Ray Laboratory, both of which are partially funded by the University, State and Commonwealth Governments.

References:

1. K. C. Wincewicz and J. S. Cooper, *J. Power Sources*, 2005, **140**, 280-296.
2. D. J. L. Brett, A. Atkinson, N. P. Brandon and S. J. Skinner, *Chem. Soc. Rev.*, 2008, **37**, 1568-1578.
3. M. K. Mahapatra and K. Lu, *J. Power Sources*, 2010, **195**, 7129-7139.
4. J. W. Fergus, *J. Power Sources*, 2005, **147**, 46-57.
5. K. A. Nielsen, M. Solvang, S. B. L. Nielsen, A. R. Dinesen, D. Beeaff and P. H. Larsen, *J. Eur. Ceram. Soc.*, 2007, **27**, 1817-1822.
6. Y. S. Chou, J. W. Stevenson and P. Singh, *J. Power Sources*, 2005, **152**, 168-174.
7. S. Ghosh, A. Das Sharma, P. Kundu and R. N. Basu, *J. Electrochem. Soc.*, 2008, **155**, B473-B478.
8. T. Zhang, Q. Zou, F. R. Zeng, S. R. Wang, D. Tang and H. W. Yang, *J. Power Sources*, 2012, **216**, 1-4.
9. T. Zhang, W. G. Fahrenholtz, S. T. Reis and R. K. Brow, *J. Am. Ceram. Soc.*, 2008, **91**, 2564-2569.
10. T. Komatsu, K. Watanabe, M. Arakawa and H. Arai, *Journal of Power Sources*, 2009, **193**, 585-588.
11. H. Kishimoto, N. Sakai, K. Yamaji, T. Horita, Y. P. Xiong, M. E. Brito and H. Yokokawa, *J. Mater. Sci.*, 2009, **44**, 639-646.
12. X. D. Zhou, J. W. Templeton, Z. Zhu, Y. S. Chou, G. D. Maupin, Z. Lu, R. K. Brow and J. W. Stevenson, *J. Electrochem. Soc.*, 2010, **157**, B1019-B1023.
13. K. Sasaki, K. Haga, T. Yoshizumi, D. Minematsu, E. Yuki, R. Liu, C. Uryu, T. Oshima, T. Ogura, Y. Shiratori, K. Ito, M. Koyama and K. Yokomoto, *Journal of Power Sources*, 2011, **196**, 9130-9140.
14. K. F. Chen, N. Ai, L. Zhao and S. P. Jiang, *J. Electrochem. Soc.*, 2013, **160**, F183-F190.
15. K. F. Chen, N. Ai, L. Zhao and S. P. Jiang, *J. Electrochem. Soc.*, 2013, **160**, F301-F308.
16. K. F. Chen, J. Hyodo, L. Zhao, N. Ai, T. Ishihara and S. P. Jiang, *J. Electrochem. Soc.*, 2013, **160**, F1033-F1039.
17. K. Chen, N. Ai, C. Lievens, J. Love and S. P. Jiang, *Electrochem. Commun.*, 2012, **23**, 129-132.
18. L. Zhao, J. J. Hyodo, K. F. Chen, N. Ai, S. Amarasinghe, T. Ishihara and S. P. Jiang, *J. Electrochem. Soc.*, 2013, **160**, F682-F686.
19. K. Chen, N. Ai and S. P. Jiang, *Fuel Cells*, 2013, **13**, 1101-1108.
20. M. J. Pascual, A. Guillet and A. Duran, *J. Power Sources*, 2007, **169**, 40-46.
21. A. Goel, M. J. Pascual and J. M. F. Ferreira, *Int. J. Hydrog. Energy*, 2010, **35**, 6911-6923.
22. D. Godeke and U. Dahlmann, *J. Power Sources*, 2011, **196**, 9046-9050.
23. S. P. Jiang, Y. D. Zhen, S. Zhang, A. I. Y. Tok and P. Wu, *J. Electrochem. Soc.*, 2006, **153**, A2120-A2125.
24. D. Tulyaganov, A. Reddy, V. Kharton and J. Ferreira, *J. Power Sources*, 2013, **242**, 486-502.
25. K. Knoblochova, H. Ticha, J. Schwarz and L. Tichy, *Optical Materials*, 2009, **31**, 895-898.
26. S. Bale, N. Rao and S. Rahman, *Solid State Sciences*, 2008, **10**, 326-331.
27. S. Bale, S. Rahman, A. Awasthi and V. Sathe, *Journal of Alloys and Compounds*, 2008, **460**, 699-703.
28. R. Vijaya Kumar, P. Gayathri Pavani, B. Ramesh, M. Shareefuddin and K. Siva Kumar, *Optical Materials*, 2013, **35**, 2267-2274.
29. X. Zhu, C. Mai and M. Li, *Journal of Non-Crystalline Solids*, 2014, **388**, 55-61.
30. Y. H. Sun and S. C. Barton, *J. Electroanal. Chem.*, 2006, **590**, 57-65.
31. B. Tiwari, A. Dixit and G. Kothiyal, *International Journal of Hydrogen Energy*, 2011, **36**, 15002-15008.
32. H. Fan, G. Gao, G. Wang and L. Hu, *Solid State Sciences*, 2010, **12**, 541-545.
33. J. L. Chen, H. W. Yang, R. Chadeyron, D. Tang and T. Zhang, *Journal of the European Ceramic Society*, 2014, **34**, 1989-1996.
34. T. Sun, H. Xiao, W. Guo and X. Hong, *Ceramics International*, 2010, **36**, 821-826.
35. N. Lahl, L. Singheiser and K. Hilpert, in *SOFC-VI*, eds. S. C. Singhal and M. Dokiya, The

Electrochem. Soc., Inc., Pennington, NJ, 1999, pp. 1057-1066.
36. T. Inoue, T. Honma, V. Dimitrov and T. Komatsu, *Journal of Solid State Chemistry*, 2010, **183**, 3078-3085.
37. Y.-S. Chou, J. W. Stevenson and R. N. Gow, *Journal of Power Sources*, 2007, **168**, 426-433.
38. P. Becker, E. Libowitzky, L. Bohatý, J. Liebertz, H. Rhee, H.-J. Eichler and A. A. Kaminskii, *Physica Status Solidi (a)*, 2012, **209**, 327-334.
39. M. K. Mahapatra and K. Lu, *Materials Science & Engineering R-Reports*, 2010, **67**, 65-85.
40. L. W. Tai, M. M. Nasrallah, H. U. Anderson, D. M. Sparlin and S. R. Sehlin, *Solid State Ionics*, 1995, **76**, 273-283.
41. S. P. Jiang, *Solid State Ionics*, 2002, **146**, 1-22.
42. T. Hong, L. Zhang, F. Chen and C. Xia, *J. Power Sources*, 2012, **218**, 254-260.
43. A. Ringuede and J. Fouletier, *Solid State Ionics*, 2001, **139**, 167-177.
44. A. Esquirol, J. Kilner and N. Brandon, *Solid State Ionics*, 2004, **175**, 63-67.
45. N. Grunbaum, L. Dessemond, J. Fouletier, F. Prado, L. Mogni and A. Caneiro, *Solid State Ionics*, 2009, **180**, 1448-1452.
46. S. P. Jiang, S. Zhang and Y. D. Zhen, *J. Electrochem. Soc.*, 2006, **153**, A127-A134.
47. S. P. Jiang and X. B. Chen, *Int. J. Hydrog. Energy*, 2014, **39**, 505-531.
48. E. Konysheva, H. Penkalla, E. Wessel, J. Mertens, U. Seeling, L. Singheiser and K. Hilpert, *J. Electrochem. Soc.*, 2006, **153**, A765-A773.
49. F. Wang, K. Yamaji, D. H. Cho, T. Shimonosono, M. Nishi, H. Kishimoto, M. E. Brito, T. Horita and H. Yokokawa, *Fuel Cells*, 2013, **13**, 520-525.
50. T. Zhang and Q. Zou, *Journal of the European Ceramic Society*, 2012, **32**, 4009-4013.
51. A. A. Reddy, D. U. Tulyaganov, S. Kapoor, A. Goel, M. J. Pascual, V. V. Kharton and J. M. F. Ferreira, *RSC Advances*, 2012, **2**, 10955-10967.
52. G. Della Mea, A. Gasparotto, M. Bettinelli, A. Montenero and R. Scaglioni, *Journal of Non-Crystalline Solids*, 1986, **84**, 443-451.
53. G. Calas, L. Cormier, L. Galoisy and P. Jollivet, *Comptes Rendus Chimie*, 2002, **5**, 831-843.

Figure captions

1. Scheme of experimental setup for the investigation of boron poisoning under SOFC operating conditions. In the figure, CE represents the counter electrode and RE represents the reference electrode.
2. Thermal expansion curves of quenched glass samples.
3. (a) Raman spectra of quenched glass samples and deconvoluted spectra for (b) G0, (c) GB, and (d) GZ glasses.
4. XPS spectra of (a) B1s and (b) O1s in quenched glass samples.
5. XRD patterns of glass samples after the heat treatment at 700^{o}C for (a) 2 h and (b) 500 h.
6. Polarization curves for the O_2 reduction reaction on LSCF cathodes under cathodic current passage at 200 mA cm^{-2} and 700^{o}C for 20 h: (a) in the absence of glass, and in the presence of (b) G0, (c) GB and (d) GZ glasses.
7. Impedance responses for the O_2 reduction reaction on LSCF cathodes after the cathodic current passage at 200 mA cm^{-2} for 20 h: (a) in the absence of glass, and in the presence of (b) G0, (c) GB and (d) GZ glasses. Comparison of R_E before and after the current passage for 20 h in the absence and presence of glass is given in (e).
8. SEM micrographs of surface (left) and cross sections (right) of LSCF cathodes: (a,b) as-prepared, and after polarization under cathodic current passage at 200 mA cm^{-2} and 700^{o}C for 20 h in the presence of (c,d) G0, (e,f) GB and (g,h) GZ glasses.
9. SEM micrographs of cross sections of LSCF cathodes after the cathodic current passage at 200 mA cm^{-2} and 700^{o}C in the presence of G0 glass for 20 h on (a,b) a 28-µm-thick LSCF and (c,d) a 6-µm-thick LSCF cathode. The enlarged images of region I and II of the 6-µm-thick LSCF cathode are shown in (e) and (f), respectively.
10. SEM micrographs of a 28-µm-thick LSCF cathode under open circuit at 700 ^{o}C in the presence of G0 glass for 20 h: (a) surface and (b) interfacial region.

11. XRD patterns of (a) 28-μm-thick LSCF electrodes after the cathodic current passage at 200 mA cm^{-2} and 700^{o}C for 20 h in the presence of G0, GB and GZ glasses, and (b) a 6-μm-thick LSCF electrode after the cathodic current passage at 200 mA cm^{-2} for 20 h in the presence of G0 glass.

Figure 1.

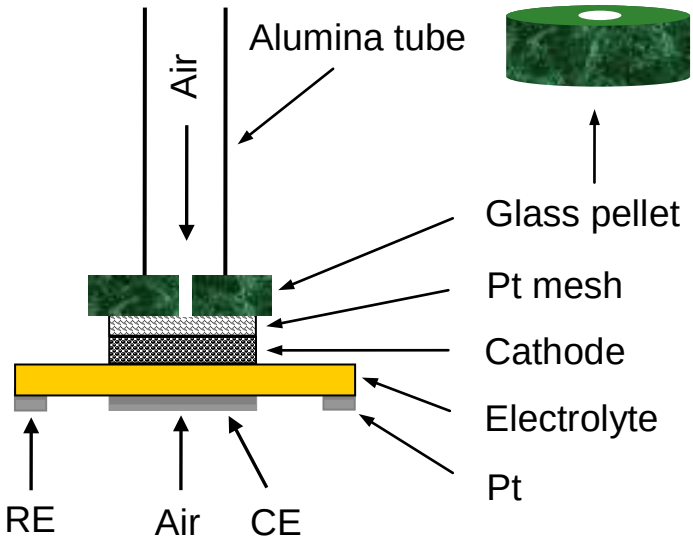

Figure 2.

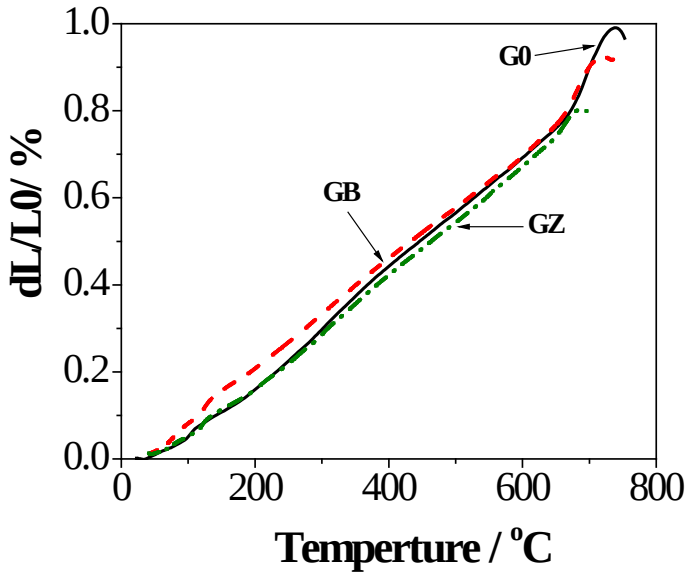

Figure 3.

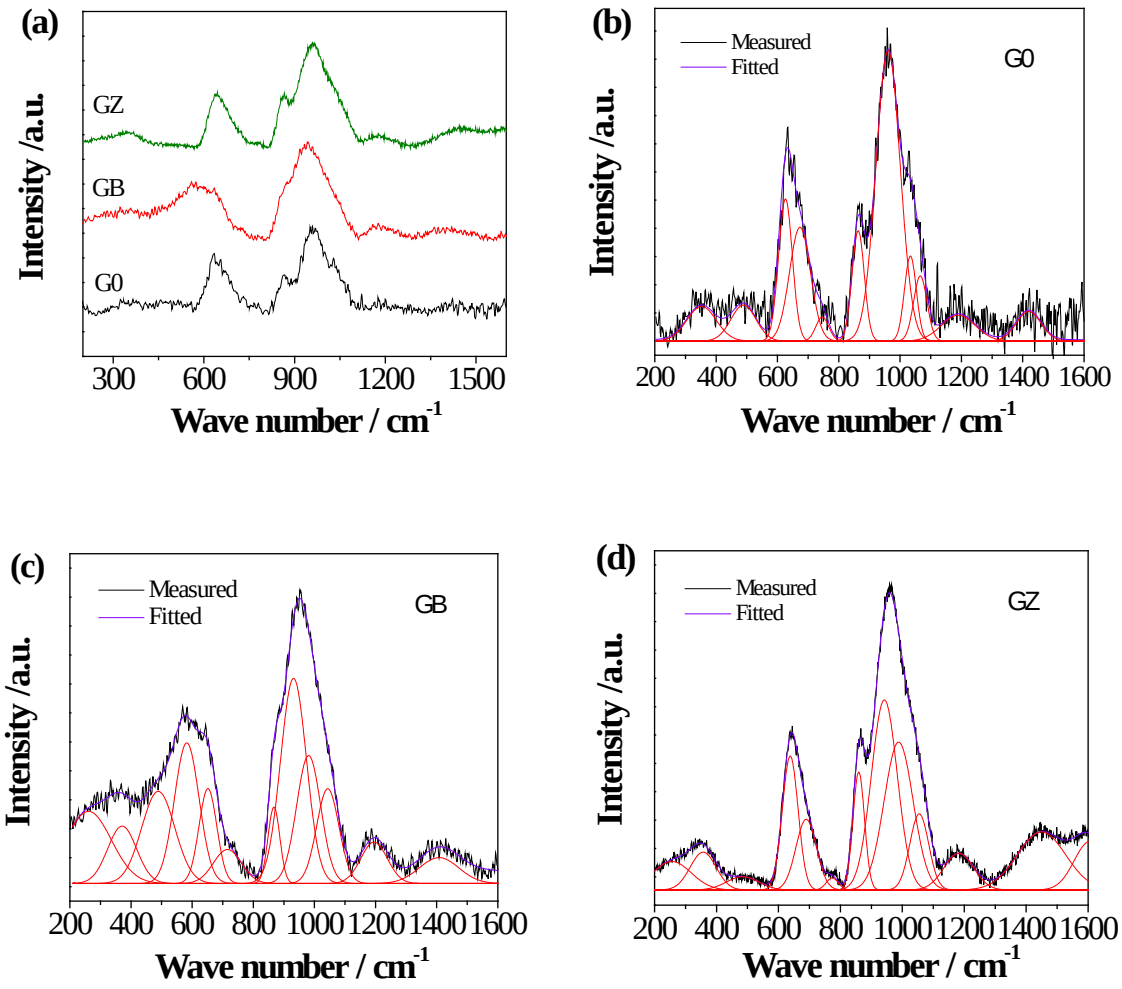

Figure 4.

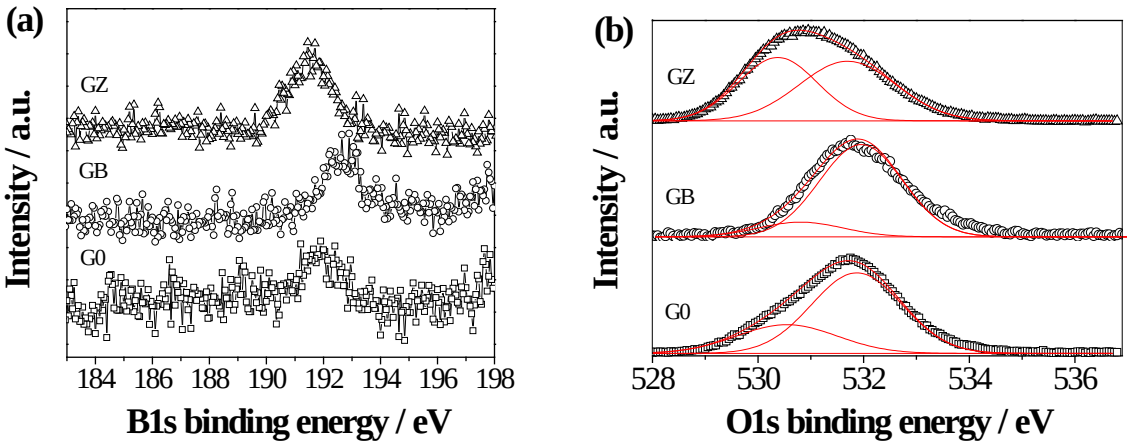

Figure 5.

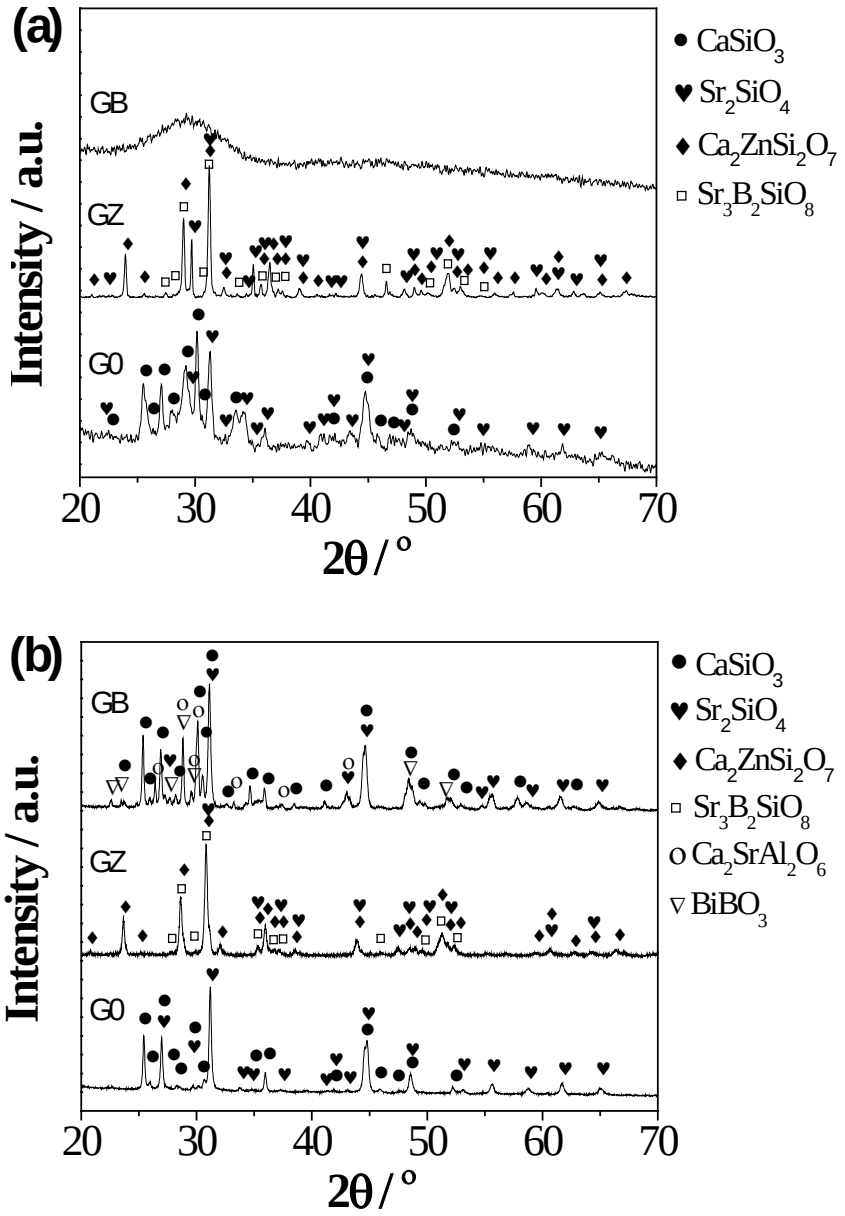

Figure 6.

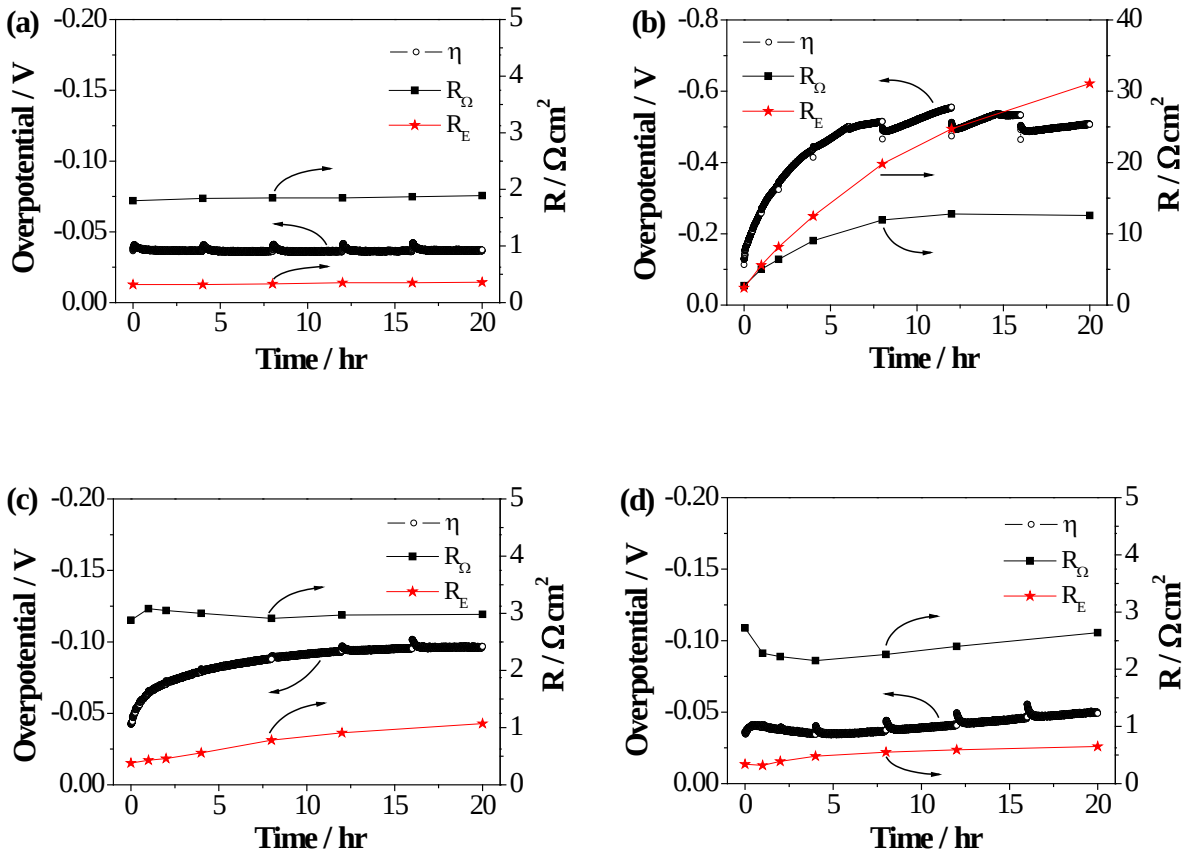

Figure 7.

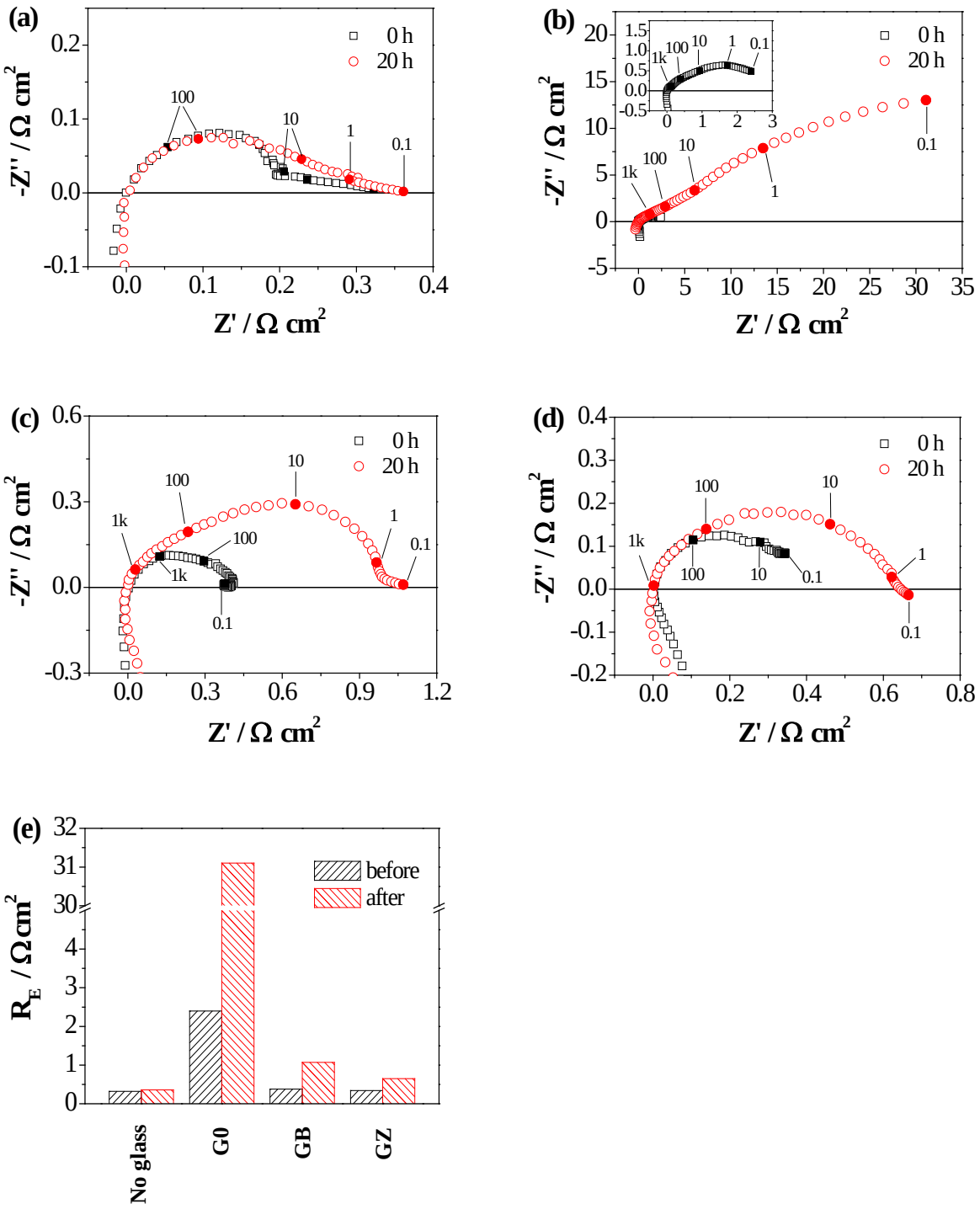

Figure 8.

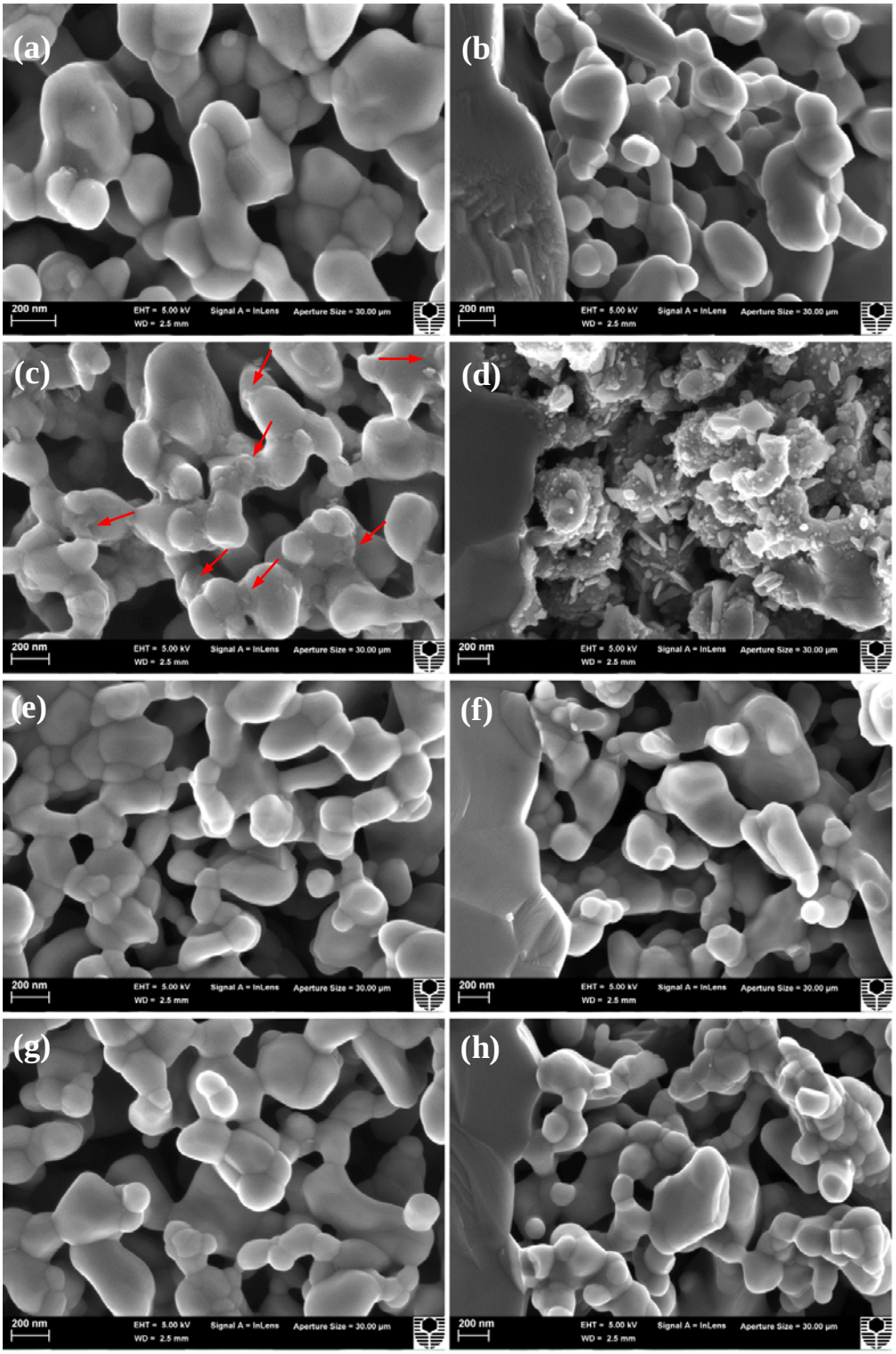

Figure 9.

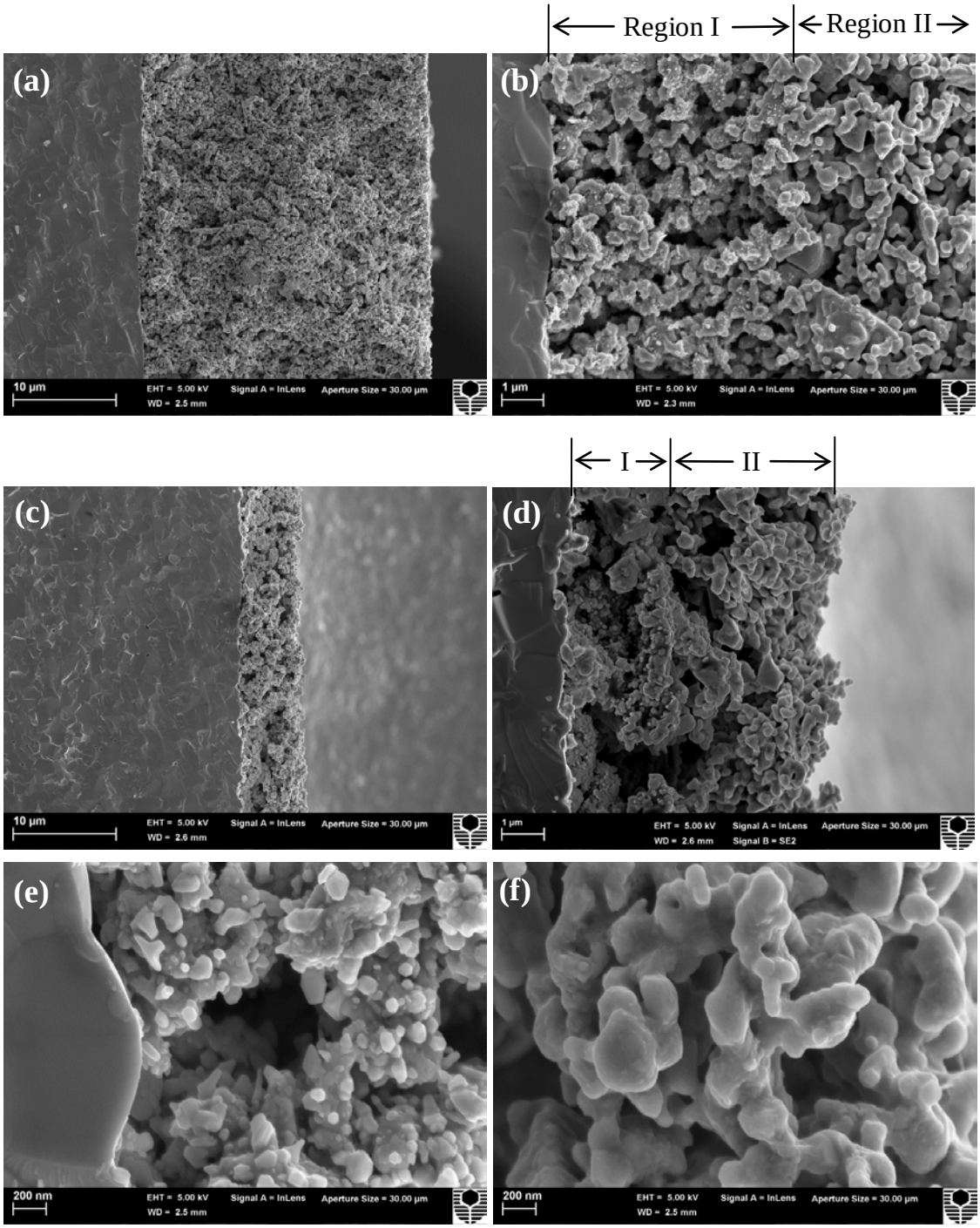

Figure 10.

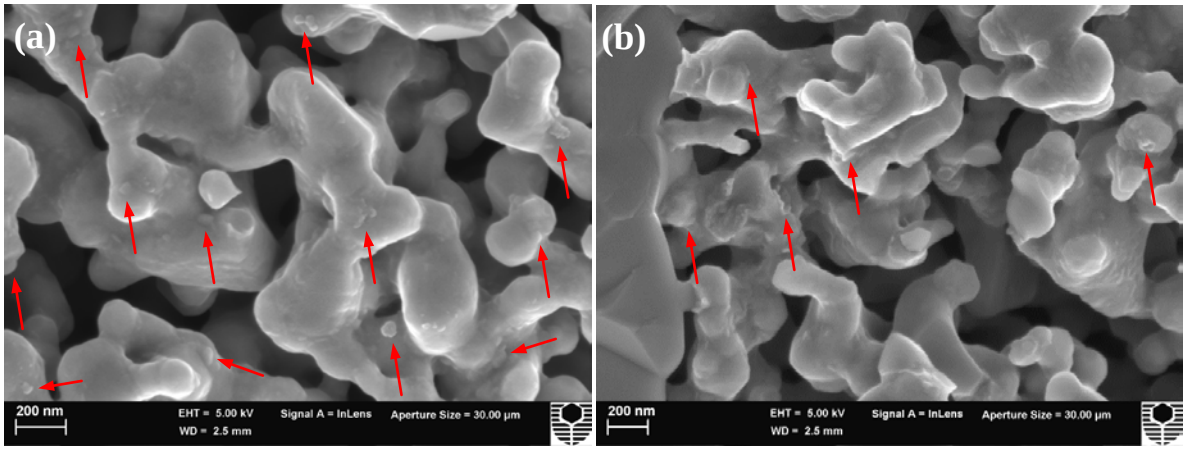

Figure 11.

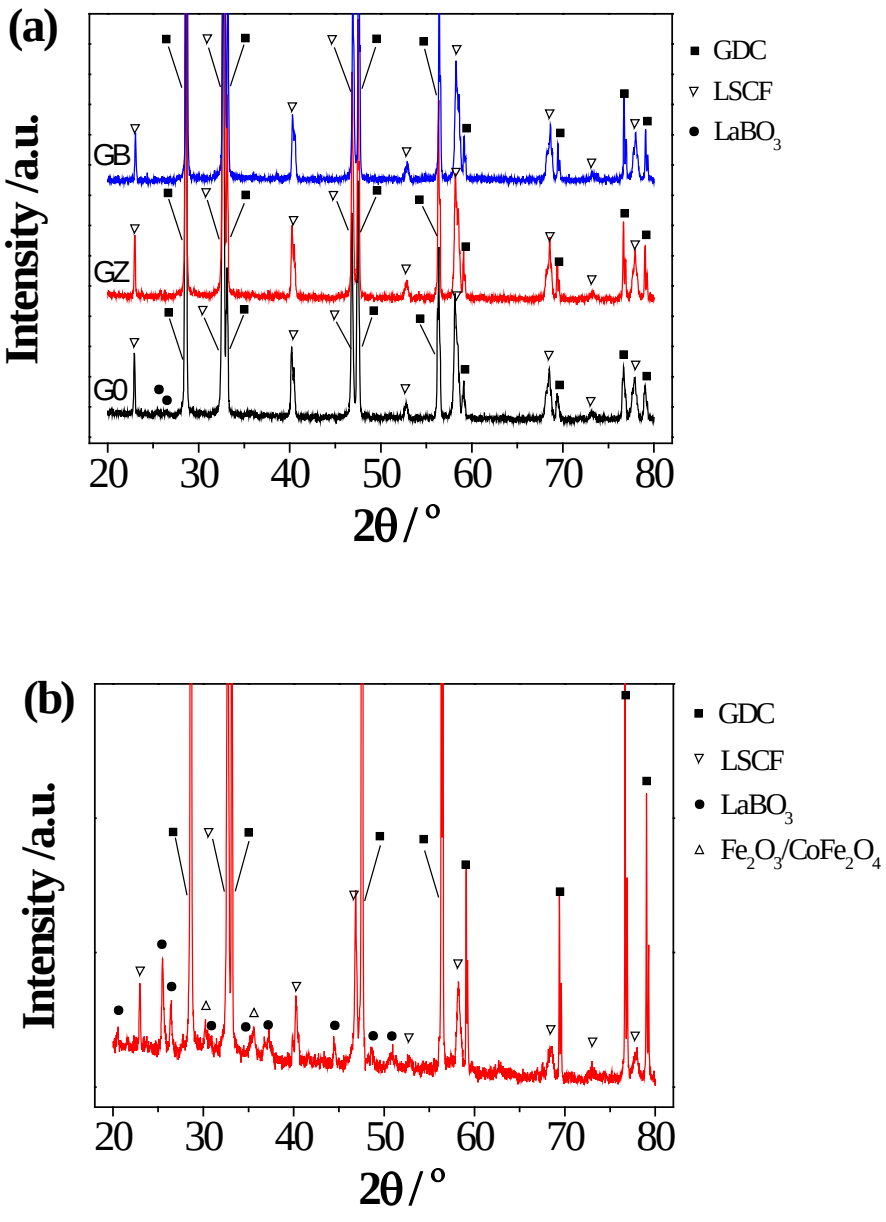

Table 1. Nominal composition of glass samples (in mole %).

Glass ID	CaO	SrO	B_2O_3	Al_2O_3	SiO_2	Bi_2O_3	ZnO
G0	26	26	8	0	40	0	0
GB	24	24	8	7	35	2	0
GZ	22	22	7	0	35	0	16

Table 2. Thermal properties of glass samples.

Glass ID	T_g (ºC)	T_d (ºC)	T_x (ºC)	CTE, as-quenched ($\times 10^{-6}$ K^{-1}, 200-600 ºC)	CTE, 700ºC for 500 h ($\times 10^{-6}$ K^{-1}, 200-600 ºC)
G0	674	739	794	13.3	12.7 ± 0.1
GB	669	722	856	12.2	10.4 ± 0.1
GZ	650	688	769	12.8	11.6 ± 0.1

Table 3. Rietveld analysis of crystallinity phases of glass samples after the heat-treatment at 700 °C for 500 h (in wt%).

	Sr_2SiO_4	$CaSiO_3$	$Ca_2ZnSi_2O_7$	$Sr_3B_2SiO_4$	$Ca_2SrAl_2O_6$	$BiBO_3$
G0	87	13	-	-	-	-
GB	21	70	-	-	4	5
GZ	9	-	84	7	-	-